doi:10.1093/brain/awaa155 BRAIN 2020: 143; 2281–2294 | 2281

BRAIN
A JOURNAL OF NEUROLOGY

Longitudinal neuroimaging biomarkers differ across Alzheimer's disease phenotypes

Irene Sintini,[1] Jonathan Graff-Radford,[2] Matthew L. Senjem,[1,3] Christopher G. Schwarz,[1] Mary M. Machulda,[4] Peter R. Martin,[5] David T. Jones,[2] Bradley F. Boeve,[2] David S. Knopman,[2] Kejal Kantarci,[1] Ronald C. Petersen,[2] Clifford R. Jack Jr,[1] Val J. Lowe,[1] Keith A. Josephs[2] and Jennifer L. Whitwell[1]

Alzheimer's disease can present clinically with either the typical amnestic phenotype or with atypical phenotypes, such as logopenic progressive aphasia and posterior cortical atrophy. We have recently described longitudinal patterns of flortaucipir PET uptake and grey matter atrophy in the atypical phenotypes, demonstrating a longitudinal regional disconnect between flortaucipir accumulation and brain atrophy. However, it is unclear how these longitudinal patterns differ from typical Alzheimer's disease, to what degree flortaucipir and atrophy mirror clinical phenotype in Alzheimer's disease, and whether optimal longitudinal neuroimaging biomarkers would also differ across phenotypes. We aimed to address these unknowns using a cohort of 57 participants diagnosed with Alzheimer's disease (18 with typical amnestic Alzheimer's disease, 17 with posterior cortical atrophy and 22 with logopenic progressive aphasia) that had undergone baseline and 1-year follow-up MRI and flortaucipir PET. Typical Alzheimer's disease participants were selected to be over 65 years old at baseline scan, while no age criterion was used for atypical Alzheimer's disease participants. Region and voxel-level rates of tau accumulation and atrophy were assessed relative to 49 cognitively unimpaired individuals and among phenotypes. Principal component analysis was implemented to describe variability in baseline tau uptake and rates of accumulation and baseline grey matter volumes and rates of atrophy across phenotypes. The capability of the principal components to discriminate between phenotypes was assessed with logistic regression. The topography of longitudinal tau accumulation and atrophy differed across phenotypes, with key regions of tau accumulation in the frontal and temporal lobes for all phenotypes and key regions of atrophy in the occipitotemporal regions for posterior cortical atrophy, left temporal lobe for logopenic progressive aphasia and medial and lateral temporal lobe for typical Alzheimer's disease. Principal component analysis identified patterns of variation in baseline and longitudinal measures of tau uptake and volume that were significantly different across phenotypes. Baseline tau uptake mapped better onto clinical phenotype than longitudinal tau and MRI measures. Our study suggests that optimal longitudinal neuroimaging biomarkers for future clinical treatment trials in Alzheimer's disease are different for MRI and tau-PET and may differ across phenotypes, particularly for MRI. Baseline tau tracer retention showed the highest fidelity to clinical phenotype, supporting the important causal role of tau as a driver of clinical dysfunction in Alzheimer's disease.

1 Department of Radiology, Mayo Clinic, Rochester, MN, USA
2 Department of Neurology, Mayo Clinic, Rochester, MN, USA
3 Department of Information Technology, Mayo Clinic, Rochester, MN, USA
4 Department of Psychiatry and Psychology, Mayo Clinic, Rochester MN, USA
5 Department of Health Science Research, Mayo Clinic, Rochester MN, USA

Correspondence to: Irene Sintini, PhD
Mayo Clinic, 200 1st St. SW, Rochester, MN 55905, USA
E-mail: Sintini.Irene@mayo.edu

Received September 26, 2019. Revised March 11, 2020. Accepted March 27, 2020. Advance access publication June 23, 2020

Keywords: longitudinal tau-PET; atrophy; Alzheimer's disease phenotypes; neuroimaging biomarkers

Abbreviations: LPA = logopenic progressive aphasia; PCA = posterior cortical atrophy; ROI = region of interest; SUVR = standard uptake value ratio

Introduction

The accumulation of tau neurofibrillary tangles and the loss of grey matter are two key biomarkers of Alzheimer's disease, which show non-random spreading patterns that differ across Alzheimer's disease clinical phenotypes (Braak and Braak, 1991; Ossenkoppele *et al.*, 2015; Jones *et al.*, 2017; Jack *et al.*, 2018; Phillips *et al.*, 2019; Sintini *et al.*, 2019). With flortaucipir PET and structural MRI, respectively, tau deposition and volume loss have been measured *in vivo* in Alzheimer's disease, both cross-sectionally (Ossenkoppele *et al.*, 2016; Jones *et al.*, 2017; Scholl *et al.*, 2017; Xia *et al.*, 2017; Whitwell *et al.*, 2018*b*) and longitudinally (Lehmann *et al.*, 2012; Rohrer *et al.*, 2013; Brambati *et al.*, 2015; Jack *et al.*, 2018; Firth *et al.*, 2019; Harrison *et al.*, 2019; Phillips *et al.*, 2019; Pontecorvo *et al.*, 2019; Rogalski *et al.*, 2019; Sintini *et al.*, 2019). In atypical Alzheimer's disease, baseline patterns of tau uptake on PET and atrophy on MRI are largely concordant and differ across phenotypes, with logopenic progressive aphasia (LPA) showing abnormalities primarily in left temporoparietal regions and posterior cortical atrophy (PCA) showing abnormalities primarily in occipitoparietal regions (Galton *et al.*, 2000; Whitwell *et al.*, 2007*a*; Ossenkoppele *et al.*, 2016; Dronse *et al.*, 2017; Xia *et al.*, 2017; Sintini *et al.*, 2018; Tetzloff *et al.*, 2018). However, we and others have shown that longitudinal patterns of tau accumulation in both atypical Alzheimer's disease phenotypes involve mostly the frontal regions while atrophy remains in posterior areas (Firth *et al.*, 2019; Sintini *et al.*, 2019). Furthermore, in atypical Alzheimer's disease, regions of the brain with high baseline tau burden and regions with high rates of tau accumulation are disconnected, with the baseline tau burden across the cortex correlating to the rates of tau accumulation in frontal and sensorimotor regions, while regions of the brain with reduced baseline grey matter volume tend to also experience more atrophy over time (Sintini *et al.*, 2019). In typical Alzheimer's disease, longitudinal tau accumulation is observed throughout the brain (Jack *et al.*, 2018), particularly in temporal regions in patients with low baseline tau burden and in parietal and frontal regions in patients with high baseline tau retention, suggesting that the amount and location of tau influence its longitudinal spread (Pontecorvo *et al.*, 2019). Longitudinal studies that have examined Alzheimer's disease cohorts consisting of both atypical and typical phenotypes have also observed longitudinal tau accumulation in the frontal lobe (Harrison *et al.*, 2019), although it is unclear whether these patterns would be observed in typical Alzheimer's disease with an old age at onset as these patients often show little tau uptake on PET (Whitwell *et al.*, 2018*a*). In contrast, atrophy spreads predominately within the medial temporal lobe and temporoparietal cortex in typical Alzheimer's disease patients (Scahill *et al.*, 2002; Whitwell *et al.*, 2007*b*; Leow *et al.*, 2009; Ossenkoppele *et al.*, 2015; Firth *et al.*, 2019). A common temporoparietal atrophy pattern has been reported across Alzheimer's disease phenotypes (Whitwell *et al.*, 2011; Ossenkoppele *et al.*, 2015). Longitudinal tau accumulation has also been investigated in Alzheimer's disease using tracers different from flortaucipir (Chiotis *et al.*, 2018; Leuzy *et al.*, 2019). Flortaucipir PET uptake has outperformed MRI measures in discriminating between Alzheimer's disease and other neurodegenerative disorders and has been advocated as a sensible instrument for differential diagnosis (Ossenkoppele *et al.*, 2018). Additionally, data-driven analysis of spatial patterns of flortaucipir PET signal across the Alzheimer's disease spectrum has revealed distinct spatial distributions that mirror the functional brain networks that support cognitive functioning impaired in Alzheimer's disease variants (Jones *et al.*, 2017).

We aimed to determine to what degree baseline and longitudinal patterns of tau-PET uptake and MRI grey matter volume loss mirror clinical phenotype in Alzheimer's disease, both by characterizing differences across clinical phenotypes and by using a data-driven principal component analysis to describe variability in each modality blinded to clinical phenotype. The overarching objective was to better understand the relationships between tau-PET, cortical volumes and neurocognitive dysfunction in Alzheimer's disease. This investigation will also allow the identification of appropriate longitudinal neuroimaging biomarkers for these Alzheimer's disease clinical phenotypes.

Materials and methods

Participants

Fifty-seven participants [18 meeting clinical criteria for amnestic dementia or typical Alzheimer's disease (McKhann *et al.*, 2011), 17 meeting clinical criteria for PCA (Crutch *et al.*, 2012) and 22 meeting clinical criteria for LPA (Gorno-Tempini *et al.*, 2011)] were recruited from the Department of Neurology between 2015 and 2019 and underwent baseline and 1-year follow-up structural MRI and flortaucipir tau-PET scans. All Alzheimer's disease participants had also undergone Pittsburgh compound B (PiB) PET imaging at baseline and were determined to be amyloid-β(+). The PCA and LPA participants had been recruited by the Neurodegenerative Research Group (NRG) and the typical Alzheimer's disease participants had been recruited into the Mayo Clinic Alzheimer's Disease Research Center. The atypical Alzheimer's disease participants analysed in this study comprised 12 PCA and 18 LPA participants that were included in a

previous study by the NRG (Sintini *et al.*, 2019). Only typical Alzheimer's disease participants over the age of 65 years at baseline scan were selected in order to ensure a more homogeneous and predominantly amnestic group. Participants were excluded from the study if they had a stroke or tumour that could explain their symptoms, if they had poor vision (20/400), if MRI was contraindicated (e.g. metal in head, cardiac pacemaker), if there were conditions that may confound brain imaging studies (e.g. structural abnormalities, including subdural haematoma or intracranial neoplasm), or if they met specific criteria for another neurodegenerative disorder, including semantic dementia, frontotemporal dementia, primary progressive apraxia of speech, corticobasal syndrome or progressive supranuclear palsy. Clinical and neuropsychological tests that were available for analysis across both cohorts included a test of general cognitive function [Montreal Cognitive Assessment Battery (MoCA)] (Nasreddine *et al.*, 2005), the Clinical Dementia Rating® Dementia Staging Instrument (CDR) (Hughes *et al.*, 1982), animal fluency (Lezak *et al.*, 2012) and the Rey-Osterrieth (Rey-O) Complex Figure test copy trial (Osterrieth, 1944). Naming was assessed with either the Boston Naming Test (BNT) (Lansing *et al.*, 1999) or the Multilingual Naming Test (MINT) (Gollan *et al.*, 2012). Memory was assessed with the Auditory-Visual Learning Test (AVLT) (Rey, 1958). Verbal fluency was assessed with the Letter fluency test (letter F only) (Loonstra *et al.*, 2001). Apolipoprotein E (*APOE*) genotyping was also performed for all participants.

Forty-nine cognitively unimpaired amyloid-β(–) individuals that had been recruited into the Mayo Clinic Study of Aging (Roberts *et al.*, 2008) and underwent the same imaging modalities as the participants were also included in the study as a control group. Forty-five of these cognitively unimpaired individuals were selected to be in the same age range as the atypical Alzheimer's disease participants [median age at baseline scan = 63 (interquartile range, IQR: 57, 72) years, 42% female, baseline Mini-Mental State Exam (MMSE) = 29 (IQR: 29, 29), follow-up MMSE = 29 (IQR: 29, 30)], while 24 (20 were overlapping) of them were selected to be in the age range of the typical Alzheimer's disease group, which was composed of older participants [median age at baseline scan = 73 (IQR: 66, 78) years, 50% female, baseline MMSE = 29 (IQR: 28, 29), follow-up MMSE = 29 (IQR: 28, 30)]. The study was approved by the Mayo Clinic IRB, and all participants provided written informed consent to participate in this study.

Image acquisition

Tau-PET scans at both time points were acquired using the same PET/CT scanner (GE Healthcare) operating in 3D mode. An intravenous bolus injection of ~370 MBq (range 333–407 MBq) flortaucipir was administered, followed by a 20 min PET acquisition performed 80 min after injection. The flortaucipir scans consisted of four 5-min dynamic frames following a low dose CT transmission scan. Standard corrections were applied. Emission data were reconstructed into a 256 × 256 matrix with a 30-cm field of view (in-plane pixel size = 1.0 mm). All participants also underwent a 3 T head MRI protocol at both timepoints that included a magnetization prepared rapid gradient echo (MPRAGE) sequence (repetition time/echo time/inversion time, 2300/3/900 ms; flip angle 8°, 26-cm field of view; 256 × 256 in-plane matrix with a phase field of view of 0.94, and slice thickness of 1.2 mm) (Jack *et al.*, 2008). A fluid-attenuated inversion recovery (FLAIR) (repetition time/echo time = 11 000/147 ms; 22-cm field of view; slice thickness = 3.6 mm) sequence was included in the MRI protocol for 48 participants. The MRI scans were performed on one of two GE scanners (GE Healthcare) with identical protocols. The MRI scans were performed a median of 1 day from the flortaucipir PET scan at both baseline and follow-up (Table 1). The baseline PiB PET scans were performed and analysed to determine amyloid-β positivity as previously described (Jack *et al.*, 2017).

Image processing

Each tau-PET image was rigidly registered to its corresponding MPRAGE using SPM12 (Wellcome Trust Centre for Neuroimaging, London, UK). Using ANTs (Avants *et al.*, 2008), the Mayo Clinic Adult Lifespan Template (MCALT, https://www.nitrc.org/projects/mcalt/) atlases (Schwarz *et al.*, 2017) were propagated to the native MPRAGE space and used to calculate regional PET values in the grey and white matter. Tissue probabilities were determined for each MPRAGE using Unified Segmentation (Ashburner and Friston, 2005) in SPM12, with MCALT tissue priors and settings (Schwarz *et al.*, 2017). Standardized uptake value ratios (SUVR) were created normalizing each tau-PET image to the cerebellar crus grey matter. PET images were not partial volume corrected in order to keep PET and MRI analyses relatively methodologically independent of each other; however, the adopted approach of masking atlas regions based on the segmentation avoids outlying voxels that are mostly non-tissue, and it thus reduces the effects of partial volume. Annualized rates of tau accumulation were calculated as the difference between the follow-up SUVR and the baseline SUVR, divided by the year difference between the two images (Chiotis *et al.*, 2018; Jack *et al.*, 2018). Eighty-four regions of interest (ROIs) covering frontal, sensorimotor, temporal, parietal and occipital lobes were selected (Sintini *et al.*, 2018) and ROI-based SUVR were calculated, using the median value. Grey matter volume was calculated in the same set of ROIs and normalized with respect to the total intracranial volume (TIV) of each participant. Annualized rates of grey matter volume loss were estimated with an in-house developed version of tensor-based morphometry using symmetric normalization (TBM-SyN), which produces annualized log Jacobian images, as previously described (Vemuri *et al.*, 2015; Sintini *et al.*, 2019). Briefly, the baseline and follow-up MPRAGE images of each subject were co-registered to their common mean. Using ANTs, we computed and applied the SyN deformation from the late to the early image, and vice versa, and averaged the deformed image with the stationary image to generate 'synthetic' early and late images. We saved the image log of the determinant of the Jacobian for the deformations, and divided them by the year difference between the two scans to get an annualized log Jacobian image. Mean annualized log Jacobian values (which can be thought as annualized percent change in grey matter volume) were calculated in each region of interest. MRI log Jacobians were not adjusted for TIV since they are unit-less. Using SPM12, PET and grey matter magnetic resonance images of each participant were subsequently spatially normalized to the MCALT template and blurred with a 6 and 8 mm full-width at half-maximum kernel, respectively, for the voxel-wise analyses. White matter hyperintensities were segmented and manually edited on the FLAIR images by a trained image analyst using a semi-automated method (Raz *et al.*, 2013).

Table 1 Demographic and clinical features of the participants

	Typical Alzheimer's disease (*n* = 18)	PCA (*n* = 17)	LPA (*n* = 22)
Female sex, *n* (%)	8 (44)	11 (65)	14 (64)
Age at baseline, years	75 (73, 80)[a,b]	65 (61, 72)	68 (62, 75)
Disease duration, years	5 (3, 7)	4 (3, 5)	2 (2, 3)[b,c]
Left handedness, *n* (%)	2 (25)[d]	3 (18)	4 (18)
Global PiB SUVR at baseline	2.59 (2.41, 3.02)	2.47 (2.29, 2.59)	2.47 (2.22, 2.97)
APOE ε4 frequency, *n* (%)	13 (76)[b]	7 (44)	9 (43)
White matter hyperintensity volume at baseline, cm^3	13.2 (11.1, 26.1)	15.8 (12.4, 23.3)	12.3 (9.8, 18.3)
Scan interval for MRI, years	1.03 (0.98, 1.09)	1.05 (0.98, 1.11)	0.99 (0.98, 1.04)
Scan interval for tau-PET, years	1.03 (0.95, 1.09)	1.06 (0.98, 1.11)	0.99 (0.98, 1.03)
Time between MRI and tau-PET baseline, days	1 (1, 7)	1 (1, 1)	1 (0, 1)
Time between MRI and tau-PET follow-up, days	1 (1, 2)	1 (1, 1)	1 (1, 1)
MoCA (/30) baseline	14 (12, 19)[b]	18 (14, 24)	20 (17, 22)
MoCA (/30) annualized change	2 (1, 5)[a,b]	4 (1, 6)	5 (4, 7)
CDR Dementia Staging Instrument (/18) baseline	4 (2, 4.5)	3 (2, 6)	1.5 (1, 2.5)[b,c]
CDR Dementia Staging Instrument (/18) annualized change	0.5 (0, 1.5)	1.5 (0.5, 2)	2 (1, 2.5)
BNT/MINT[e] % correct baseline	78 (70, 91)	67 (57, 90)	73 (55, 87)
BNT/MINT % correct annualized change	0 (–1, 9)[b]	6 (0, 14)	14 (6, 25)
AVLT[f] delayed% recall MOANS baseline	5 (4, 6)[b]	6 (5, 8)	6 (5, 12)
AVLT delayed% recall MOANS annualized change	0 (0, 1)	0 (–1, 2)	0 (–2, 3)
Animal fluency baseline	10 (9, 14)	12 (9, 17)	11 (8, 15)
Animal fluency annualized change	1 (–2, 4)	2 (1, 4)	2 (1, 4)
Rey-O MOANS[g] baseline	7 (4, 8)	2 (2, 2)[a,c]	6 (2, 10)
Rey-O MOANS annualized change	0 (–2, 0)	0 (0, 0)	0 (0, 2)
Letter fluency F baseline	11 (6, 18)	13 (10, 16)	11 (8, 12)
Letter fluency F annualized change	1 (0, 2)	0 (–3, 3)	3 (1, 5)[b,c]

Data are shown as median (IQR), or *n* (%). AVLT = Auditory-Verbal Learning Test (Rey, 1958); BNT = Boston Naming Test (Lansing *et al.*, 1999); CDR = Clinical Dementia Rating (sum of boxes) (Hughes *et al.*, 1982); MINT = Multilingual Naming Test (Gollan *et al.*, 2012); MOANS = Mayo Older American Normative scale (Ivnik *et al.*, 1992; Machulda *et al.*, 2007); MoCA = Montreal Cognitive Assessment Battery (Nasreddine *et al.*, 2005); PiB SUVR = Pittsburgh Compound B standardized uptake value ratio; Rey-O = Rey Osterrieth (Osterrieth, 1944).

[a]Typical Alzheimer's disease is statistically different from PCA ($P < 0.05$ using Students *t*-test or Fisher's exact test).

[b]Typical Alzheimer's disease is statistically different from LPA ($P < 0.05$ using Students *t*-test or Fisher's exact test).

[c]PCA is statistically different from LPA ($P < 0.05$ using Students *t*-test or Fisher's exact test).

[d]Data available for eight participants.

[e]BNT was administered for the LPA and PCA groups, while the MINT was administered to the typical Alzheimer's disease group. In order to compare across groups performance on each test is shown as % correct.

[f]AVLT delayed% recall MOANS is age-adjusted.

[g]MOANS scores are constructed to have an average of 10, standard deviation of 3, in controls.

Statistical analyses

Voxel-based statistics

Alzheimer's disease phenotypes were compared to the cognitively unimpaired individuals, and compared to each other, using multiple linear regression models in SPM12. The LPA and PCA groups were compared to the 45 cognitively unimpaired individuals that were matched to the atypical Alzheimer's disease participants, and the typical Alzheimer's disease group was compared to the 24 cognitively unimpaired individuals that were matched to the typical Alzheimer's disease participants. Age was modelled as a covariate in all analyses. SPM analyses were run on tau-PET SUVR and grey matter segmentation magnetic resonance images at baseline and follow-up as well as on annualized tau-PET SUVR change and MRI annualized log Jacobians images. SPM maps were visualized with BrainNet Viewer (Xia *et al.*, 2013).

Region-based statistics

To investigate the patterns of tau accumulation and atrophy across the phenotypes, two-sided Wilcoxon rank-sum tests were performed to identify the ROIs that best discriminated between each Alzheimer's disease phenotype and cognitively unimpaired individuals in terms of longitudinal changes. Subsequently, area under the receiver operator curve (AUROC) values were calculated. The AUROC is the probability that a positive observation (e.g. the rate of tau accumulation in a region for the Alzheimer's disease participants) is ranked higher than a negative observation (e.g. the rate of tau accumulation in the same region for the cognitively unimpaired individuals). Therefore, the higher the AUROC, the better the discrimination between groups. The *P*-values of the AUROC were adjusted for multiple comparisons using the Bonferroni method and statistical significance was set at $P < 0.05$. These analyses were performed in MATLAB 2018a (The Mathworks, Inc., Natick, MA, USA) and R (version 3.4.4; R Foundation for Statistical Computing).

Principal component analysis

Principal component analysis is a multivariate statistical technique used to identify and rank the independent modes of variation in a dataset (Jolliffe, 1986), with a completely data-driven approach. It can be used to transform a set of possibly

correlated variables into a set of uncorrelated variables, called principal components. Principal component analysis was performed on the participants' tau-PET SUVR baseline and annualized change images and ROI grey matter baseline volumes and MRI annualized log Jacobians to describe the patterns of greatest variance in the population and verify whether these patterns matched the three Alzheimer's disease phenotypes. Principal component analysis was applied to the *z*-scores of each image modality separately, using the singular value decomposition algorithm in MATLAB 2018a. *Z*-scores were computed for the Alzheimer's disease participant's tau-PET SUVR images, subtracting from each participant's image the mean of the cognitively unimpaired images and dividing by the standard deviation of the cognitively unimpaired images. The effect of age in the cognitively unimpaired group was regressed out of the Alzheimer's disease participant's images using SPM12, similar to a previous study (Ossenkoppele *et al.*, 2015). Age effects were estimated in the cognitively unimpaired individuals in this way to avoid removing specific disease-related age associations within the Alzheimer's disease cohort, as previously published (Sintini *et al.*, 2019). Similarly, *z*-scores were computed for the ROI grey matter baseline volumes (Phillips *et al.*, 2018) and MRI annualized log Jacobians and the effect of age in the cognitively unimpaired group was regressed out of the participants' regional quantities. To visualize the variability that the voxel-based and ROI-based principal components captured, brain maps were reconstructed using the 5th and 95th percentile of each tau-PET uptake principal component and Pearson's *R* correlation coefficients between each principal component and each ROI volume and MRI annualized log Jacobian were calculated, respectively. Only the first four principal components are reported, as they explained most of the variability in the population and the subsequent principal components were associated with more subtle patterns. Statistical differences between the principal components of the three clinical phenotypes were assessed with unpaired *t*-tests. To examine the effect of disease severity on the imaging patterns that the principal component analyses uncovered, Pearson's *R* correlation coefficients were calculated between principal component scores of each modality and baseline MoCA scores, as a quantitative measure of disease severity.

Penalized multinomial logistic regression was used to assess the capability of the principal components to discriminate between clinical phenotypes, as described in a previous study (Josephs *et al.*, 2018). The elastic net technique was used in the logistic regression models for regularization. Models were fit within each modality (tau-PET SUVR baseline and annualized change images; ROI grey matter baseline volumes and MRI annualized log Jacobians) with increasing numbers of principal components, from two up to 15 principal components, which explained a cumulative variation of at least 80% in every modality. The fidelity of the different imaging modalities to the clinical phenotypes was compared using the per cent of participants correctly classified into their phenotype by the logistic regression models. These analyses were performed using *R* version 3.6.0.

Data availability

Data that support the findings in this study area available from the corresponding author upon reasonable request.

Results

Demographic and clinical findings

By design, the typical Alzheimer's disease group was older than the PCA ($P = 0.0001$) and LPA ($P = 0.0006$) groups (Table 1). The LPA group had shorter disease duration than typical Alzheimer's disease ($P = 0.001$) and PCA ($P = 0.04$). There were more *APOE* ε4 carriers in typical Alzheimer's disease compared to LPA ($P = 0.05$) and PCA ($P = 0.08$). Typical Alzheimer's disease participants performed worse on baseline MoCA ($P = 0.04$) than LPA and declined less than LPA ($P = 0.02$) and PCA ($P = 0.05$). LPA participants had lower baseline CDR than PCA ($P = 0.04$) and typical Alzheimer's disease ($P = 0.04$). LPA participants declined more on MINT/BNT % correct ($P = 0.007$) and performed better on baseline AVLT delayed% recall MOANS ($P = 0.02$) than typical Alzheimer's disease. PCA participants performed worse on the Rey-O Complex Figure at baseline compared to LPA ($P = 0.002$) and typical Alzheimer's disease ($P = 0.001$). LPA participants declined more than PCA ($P = 0.02$) and typical Alzheimer's disease ($P = 0.04$) on the Letter fluency test. No differences were observed between groups in the severity of white matter hyperintensities.

Comparisons across Alzheimer's disease phenotypes

Baseline and follow-up patterns of tau uptake and grey matter volume loss are shown in the Supplementary material and were largely consistent with expected regional distributions in the Alzheimer's disease phenotypes when compared to cognitively unimpaired individuals, with left temporoparietal abnormalities observed in LPA, occipitoparietal abnormalities in PCA and medial temporal with milder temporoparietal abnormalities in typical Alzheimer's disease (Supplementary Fig. 1). Similar to what we have previously reported (Sintini *et al.*, 2019), the LPA and PCA participants showed increased rates of tau accumulation predominantly in the frontotemporal (PCA, LPA) and parietal (LPA) lobe, with increased rates of atrophy in the occipitotemporal (PCA) and left temporal (LPA) lobe compared to cognitively unimpaired individuals (Fig. 1). The typical Alzheimer's disease participants showed increased rates of atrophy mostly in the temporal regions and did not show any regions with increased rates of tau accumulation after correction for multiple comparisons, although at an uncorrected threshold increased rates of tau accumulation were observed in the right occipital, right lateral temporal and bilateral frontal regions (Fig. 1). Unthresholded maps relative to cognitively unimpaired are reported in Supplementary Fig. 2.

Comparisons of patterns of cross-sectional tau-PET uptake and grey matter volume loss among phenotypes are shown in the Supplementary material as uncorrected maps at $P < 0.001$. Cross-sectionally at baseline and follow-up, LPA participants showed elevated tau-PET uptake in the left

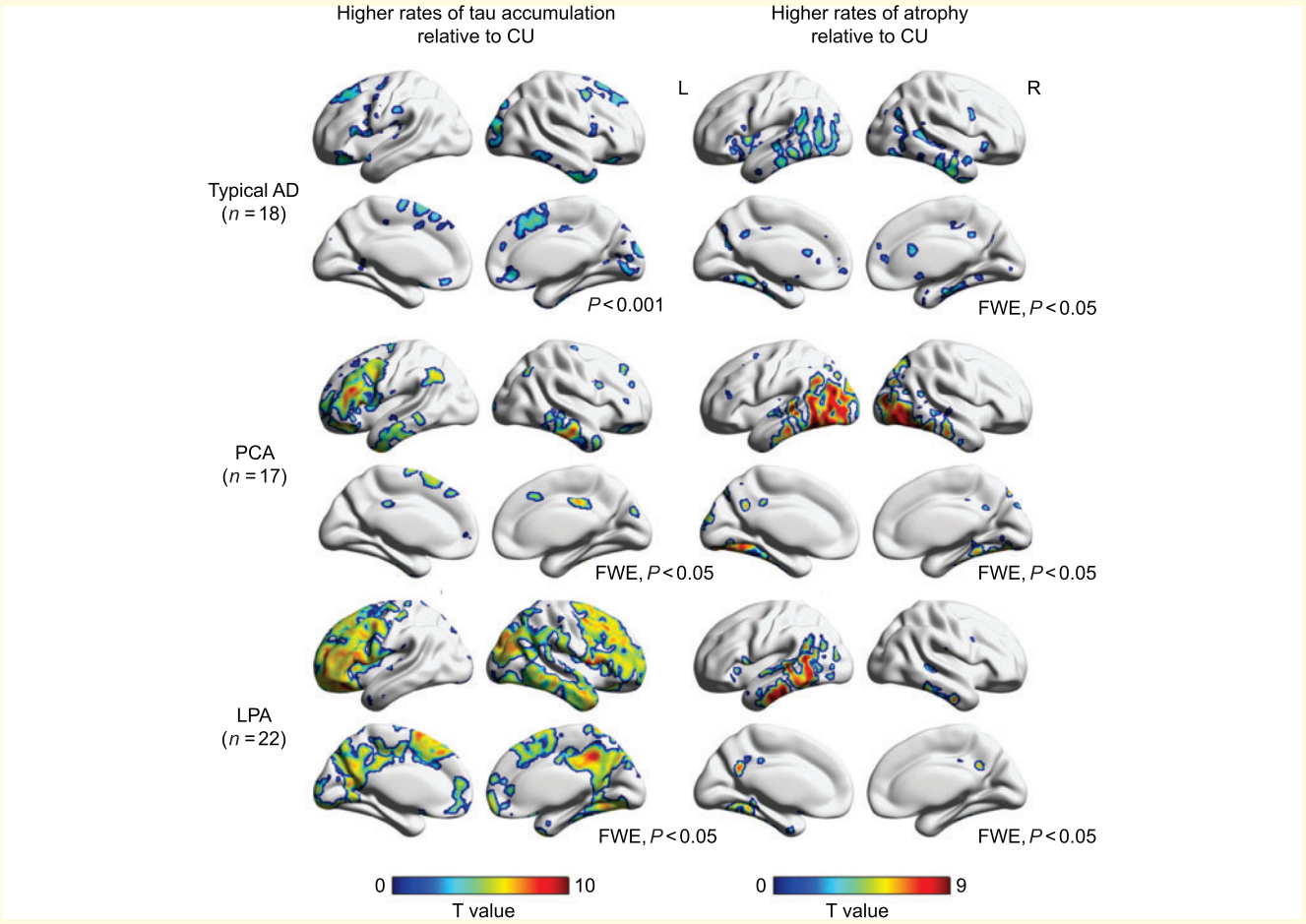

Figure 1 Longitudinal tau-PET uptake and atrophy patterns in Alzheimer's disease phenotypes. SPM maps of higher annualized rates of tau-PET uptake accumulation and of atrophy (i.e. MRI annualized log Jacobians) for typical Alzheimer's disease (AD), PCA and LPA participants relative to cognitively unimpaired (CU). Results are shown after FWE correction for multiple comparison ($P < 0.05$), except for the typical Alzheimer's disease rates of atrophy map, which is shown uncorrected ($P < 0.001$).

temporoparietal and frontal regions and reduced grey matter volume in the left temporal regions compared to PCA, while PCA participants showed elevated tau-PET uptake and reduced grey matter volumes in the right occipital regions relative to LPA (Supplementary Fig. 3). Typical Alzheimer's disease participants showed elevated tau-PET uptake and reduced grey matter volume in the right medial temporal lobe relative to LPA (Supplementary Fig. 3). Typical Alzheimer's disease participants also showed elevated tau-PET uptake in frontal regions, and lower tau-PET uptake and higher grey matter volume in bilateral occipital regions relative to PCA (Supplementary Fig. 3). Longitudinally, LPA showed higher rates of tau accumulation than PCA in the right temporoparietal regions, while PCA showed higher rates of atrophy than LPA in bilateral occipital regions (Supplementary Fig. 4). Very few voxels survived when typical Alzheimer's disease longitudinal measures were compared to PCA and LPA (Supplementary Fig. 4).

Longitudinal ROI biomarkers

The ROIs whose annual rates of tau accumulation best discriminated between the Alzheimer's disease participants and cognitively unimpaired individuals were predominantly frontal and temporal lobe regions for all three Alzheimer's disease phenotypes (Fig. 2A). The ROIs with the highest AUROC for typical Alzheimer's disease participants were in the right temporal lobe followed by regions in the bilateral frontal and occipital lobes, which did not survive correction for multiple comparisons. PCA and LPA participants showed the highest annual rates of tau accumulation relative to cognitively unimpaired in the left frontal and bilateral temporal lobes and in the left frontal and right temporal lobes, respectively. Relevant ROIs were also found in the parietal lobe for LPA and sensorimotor for PCA. The ROIs whose rates of atrophy best discriminated between Alzheimer's disease participants and cognitively unimpaired individuals were bilateral medial

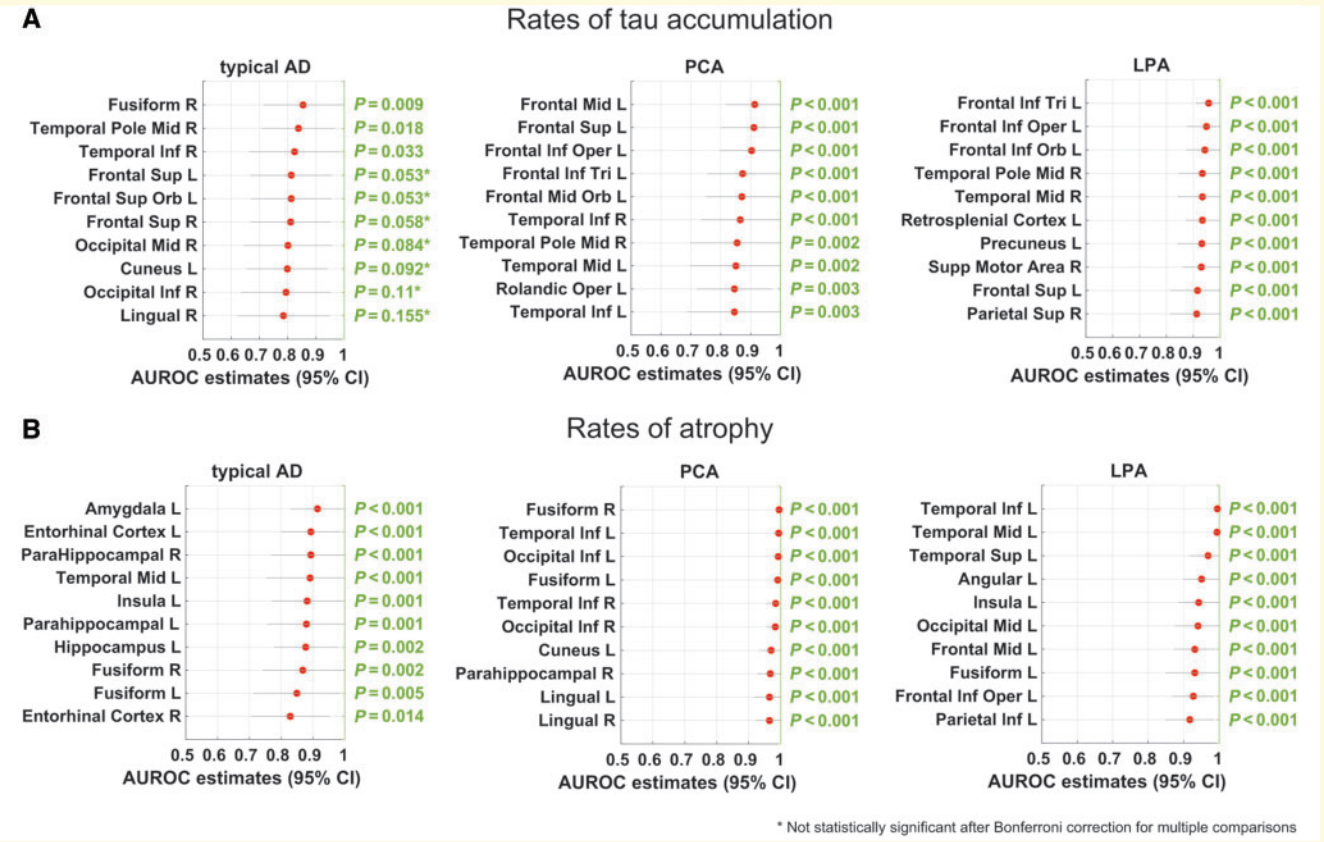

Figure 2 AUROC estimates of longitudinal regional measures. AUROC estimates for each Alzheimer's disease (AD) phenotype against cognitively unimpaired individuals. AUROC were calculated using ROI-based rates of tau accumulation (**A**) and atrophy (**B**). ROIs are listed according to a decreasing order of their AUROC and only the first 10 regions are reported. The reported *P*-values were adjusted for multiple comparisons using the Bonferroni method. CI = confidence interval.

temporal lobe regions for typical Alzheimer's disease and inferior temporal and fusiform regions for both PCA and LPA (Fig. 2B). Additional ROIs were the left insula for typical Alzheimer's disease and LPA, the occipital lobe regions for PCA, and the left frontal, left occipital and left parietal regions for LPA.

Principal component analysis

Voxel-based variability in tau uptake in Alzheimer's disease as described by the first four principal components is shown in Fig. 3. For baseline tau uptake, PC1 captured 49% of the variability in the population and described severity of uptake in the temporal, parietal and occipital lobes (Fig. 3A). PC2 (17%) and PC3 (6%) described bilateral occipital tau uptake (PC2, 95th percentile) versus temporal, parietal and frontal uptake, particularly on the left (PC2, 5th percentile) and right occipital uptake (PC3, 95th percentile) versus left occipitotemporal uptake (PC3, 5th percentile), respectively. PC4 (5%) described a pattern of variability that was common across phenotypes: bilateral occipitoparietal uptake (PC4, 95th percentile) versus bilateral occipitotemporal uptake (PC4, 5th percentile). For rate of tau accumulation, PC1 (41%) described severity of tau accumulation throughout the brain, particularly in the temporal, parietal and occipital regions (Fig. 3B). PC2 (7%) and PC3 (5%) described patterns of tau accumulation in bilateral frontal regions (PC2, 5th percentile) versus right temporoparietal regions (PC2, 95th percentile) and in left temporal and parietal regions (PC3, 5th percentile) versus right occipital regions (PC3, 95th percentile), respectively. PC4 (5%) described a pattern of tau accumulation in the left occipital lobe (PC4, 95th percentile) versus the right temporoparietal and left frontal regions (PC4, 5th percentile).

ROI-based variability in MRI grey matter volume in Alzheimer's disease as described by the first four principal components is shown in Fig. 4. Only statistically significant correlations ($P < 0.05$) were reported. For baseline grey matter volumes, PC1 (26%) was proportional to volumes across the brain, with an emphasis on posterior regions, while PC2 (12%) was proportional to medial temporal volumes. Baseline grey matter volume PC1 and PC2 were the only principal components that had a mild correlation with baseline MoCA score ($R = 0.25$ for both, $P = 0.06$), that is participants with a higher baseline MoCA score tended to have larger grey matter volumes. PC3 (7%) was proportional to frontal and sensorimotor

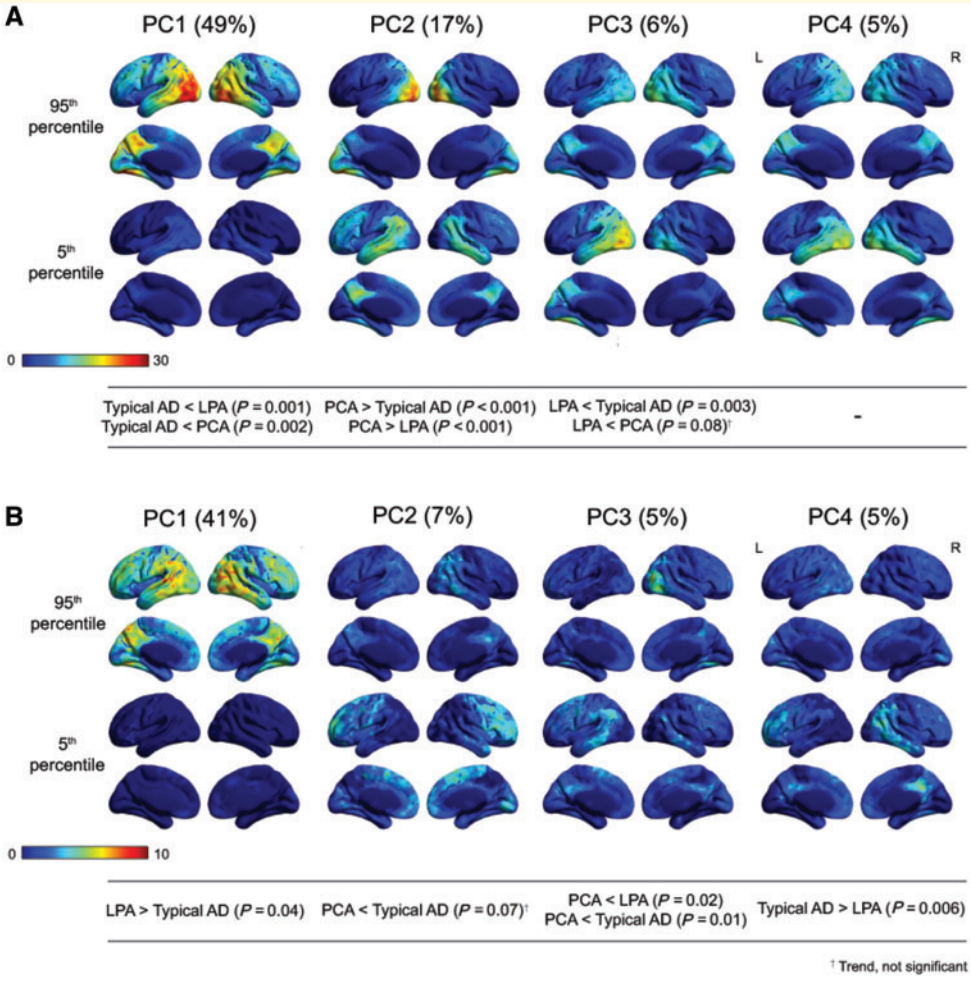

Figure 3 Principal component analyses of tau-PET uptake. Variability in baseline tau-PET uptake (**A**) and annualized rates of tau accumulation (**B**) as described by the first four principal components. To visualize the variability captured by the principal components, brain maps were reconstructed using the 5th and 95th percentile of each principal component. For example, from **A**, a participant with a high PC2 score (i.e. closer to the 95th percentile) has high lateral occipital uptake, while a participant with a low PC2 score (i.e. closer to the 5th percentile) has high lateral temporal uptake. The tables below the brain maps show which phenotypes have statistically different principal component scores. For example, from **A**, PC2 is statistically higher for PCA participants, meaning that PCA participants will resemble more the 95th percentile map of PC2, while LPA and typical Alzheimer's disease (AD) will resemble more the 5th percentile map of PC2.

volumes and inversely proportional to occipital volumes. PC4 (5%) was inversely proportional to right occipital and bilateral frontal volumes and proportional to left temporal volumes. For rates of atrophy estimated with MRI annualized log Jacobians, PC1 (47%) was inversely proportional to rates of atrophy, i.e. proportional to MRI log Jacobians, throughout the brain. PC2 (10%) was proportional to atrophy in the frontal lobes and inversely proportional to atrophy in the sensorimotor and parietal regions. PC3 (7%) was inversely proportional to atrophy in the occipital regions. PC4 (6%) was inversely proportional to atrophy in the left temporal and right parietal regions, and proportional to atrophy in the right frontal regions.

The penalized logistic regression models showed that principal components from baseline tau-PET uptake measurements outperformed the other modalities in their fidelity to the specific neurocognitive dysfunction exhibited by the three syndromes, when using the first two (70% correctly classified) to five (77%) principal components (Fig. 5). Baseline MRI principal components did not do as well. Sixty percent of the participants were correctly classified by the logistic regression model fitted on the first two principal components from baseline MRI volume measures. This result went up to 68% using three principal components and to 89% using 15 principal components. Models based on longitudinal measurements performed worse with low numbers of principal components, with $<40\%$ of participants correctly classified using the first two principal components, but reached similar outcomes to the models based on baseline measures as the number of principal components increased:

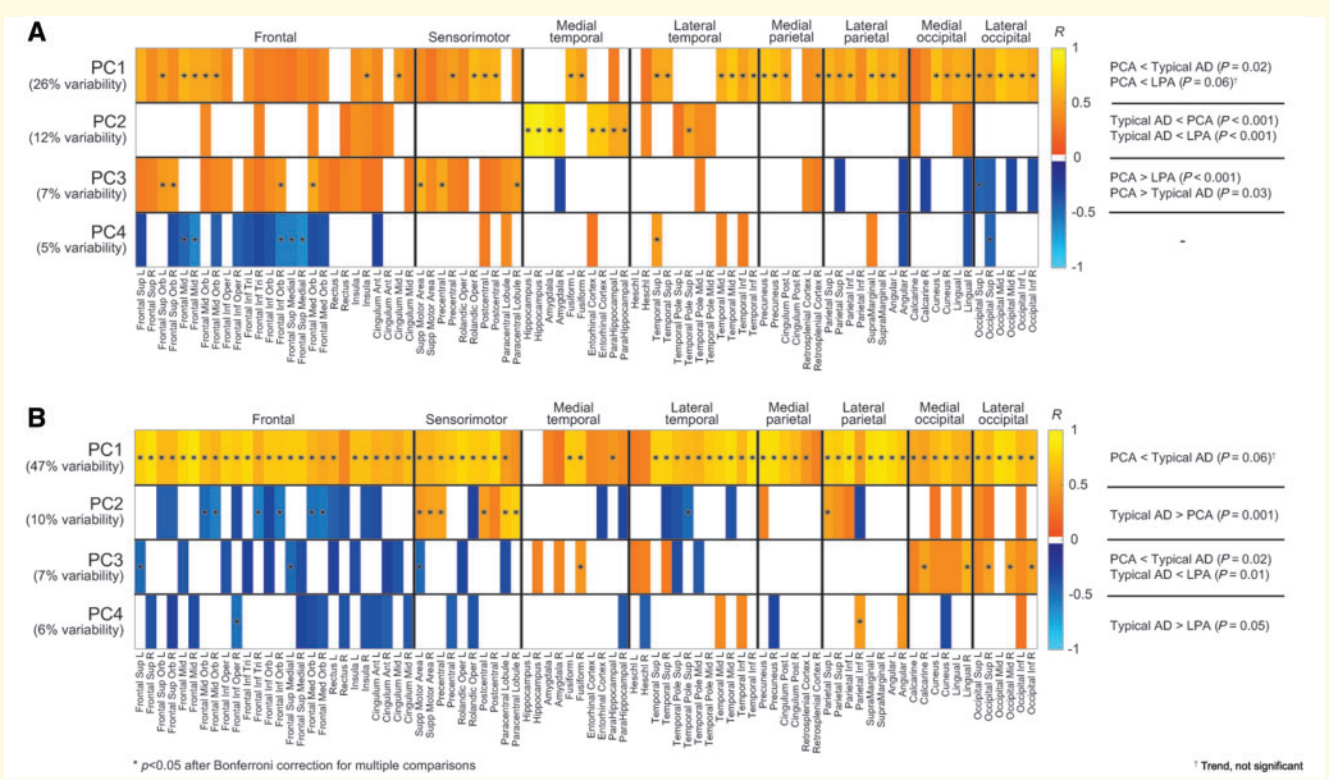

Figure 4 Principal component analyses of grey matter volumes. Variability in baseline MRI grey matter volumes (**A**) and MRI annualized log Jacobians (**B**) as described by the first four principal components. To visualize the variability captured by the principal components, the Pearson's *R* correlation coefficients between each principal component and each regional volume (**A**) and log Jacobian (**B**) are reported. For example, from **A**, a participant with a high PC2 score has high volumes in the medial temporal regions. Only correlations with $P < 0.05$ are shown. Correlations that survived Bonferroni correction for multiple comparisons at $P < 0.05$ are marked with an asterisk. The tables on the right show which phenotypes have statistically different principal component scores. For example, from **A**, PC2 is statistically lower for typical Alzheimer's disease (AD) participants, meaning that they have lower medial temporal grey matter volumes than PCA and LPA participants.

77% and 78% of participants were correctly classified with eight principal components for rates of tau accumulation and with 14 principal components for rates of atrophy, respectively.

Discussion

In this study, we investigated the variability in the spatial patterns of tau burden and atrophy across the typical (amnestic) and atypical (visual dysfunction and logopenic aphasic) Alzheimer's disease clinical spectrum and the fidelity with which such patterns mirrored clinical dysfunction in Alzheimer's disease. Specifically, we used baseline and rate of change measures from flortaucipir PET uptake and structural MRI, with the goal of finding variant-specific imaging biomarkers and quantifying and comparing the ability of these imaging modalities to discriminate between Alzheimer's disease clinical phenotypes. We found that, not only do the baseline patterns of tau and atrophy differ across phenotypes, but each phenotype presented its unique longitudinal regional patterns of disease progression on tau-PET and MRI, with some commonalities. Frontal tau accumulation appeared to be a specific biomarker for the two atypical Alzheimer's disease variants, with the temporal lobes being additional key regions of change characterized by high AUROC estimates for differentiating PCA and LPA from cognitively unimpaired individuals. This finding strengthens the idea of a disease spreading from the regions that are most affected at baseline to new regions of the brain (Sintini *et al.*, 2019), that is, from the left temporal lobe primarily into the left frontal, right temporal and parietal lobes for LPA and from the occipital lobe into the left frontal and bilateral temporal lobes in PCA. Although frontal regions also showed tau accumulation over time in typical Alzheimer's disease, the annual rates were milder in this phenotype and the AUROC estimates differentiating typical Alzheimer's disease from cognitively unimpaired individuals were lower, suggesting that annual rates of tau accumulation would be a more efficient outcome measure in trials of atypical than in typical Alzheimer's disease. Longitudinal MRI biomarkers differed from the tau-PET ones. Atrophy in bilateral occipitotemporal regions provided optimal biomarkers in PCA (i.e. biomarkers that best differentiate between PCA and cognitively unimpaired), and left temporal

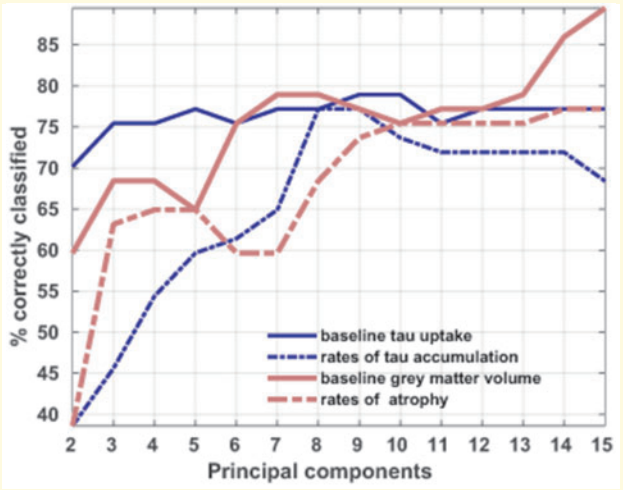

Figure 5 Diagnostic power of principal components. Diagnostic power of each imaging modality estimated by how many participants were classified into their correct phenotype using penalized multinomial regression models based on increasing numbers of principal components.

and parietal regions provided optimal biomarkers in LPA. Our analysis confirmed the sparing of the hippocampus from neurodegeneration in atypical Alzheimer's disease (Phillips *et al.*, 2018; Firth *et al.*, 2019) as the disease progresses, while the medial temporal regions were identified as the key regions of atrophy in typical Alzheimer's disease (Firth *et al.*, 2019). The left middle and inferior temporal regions performed well as a biomarker across all three phenotypes, suggesting that atrophy in this region may be specific to Alzheimer's disease and less related to specific cognitive symptoms. It is possible that this region, or Braak-like tau patterns in general (Jones *et al.*, 2017), could be a useful general biomarker for clinical treatment trials that enrol these different clinical phenotypes of Alzheimer's disease, although further analysis will be needed to confirm this hypothesis.

The baseline and longitudinal patterns of tau uptake and atrophy presented here further confirm and strengthen what we and others have found in typical and atypical Alzheimer's disease studies. However, in the current work, the larger and more diverse patient population allowed us to investigate variation in neuroimaging measures across Alzheimer's disease phenotypes, employing a data-driven, unsupervised statistical technique that is principal component analysis, which identifies patterns of variation in the data, without relying on clinical diagnosis. Each principal component explains part of the variance in the dataset and can be seen as a predictor in diagnostic research (Pagani *et al.*, 2009). Principal component analysis has been successfully applied to voxel (Zuendorf *et al.*, 2003) and ROI (Pagani *et al.*, 2009; Josephs *et al.*, 2018) level data to describe the patterns of greatest variance within a population and discriminate between participants groups. Other related data-driven approaches have been successfully applied voxel-wise to tau-PET data (Jones *et al.*, 2017; Vogel *et al.*, 2019). We found that the principal components from both the tau-PET and MRI baseline data were reflective of Alzheimer's disease phenotypes. The first component, which explains the largest degree of variability, captured general severity across the cortex and it differentiated typical Alzheimer's disease from PCA and LPA in baseline tau uptake, with typical Alzheimer's disease showing less severe cortical tau uptake. This is likely due in part to the fact that the typical Alzheimer's disease participants in this study were older than the atypical Alzheimer's disease participants, with previous studies showing that older age is associated with less cortical tau uptake and atrophy in Alzheimer's disease (Frisoni *et al.*, 2005; Jones *et al.*, 2017; Scholl *et al.*, 2017; Lowe *et al.*, 2018; Whitwell *et al.*, 2018*a*, 2019). The subsequent components captured more phenotype-specific patterns. The second and third principal components from baseline tau-PET uptake were specific for PCA (occipital tau uptake) and LPA (left temporal tau uptake), respectively. On the contrary, principal component analysis of baseline grey matter volume identified a specific principal component for typical Alzheimer's disease (PC2), which captured variability in the medial temporal volumes. The fact that a medial temporal component was only identified on MRI might be due to the older age of the typical Alzheimer's disease participants, which increases the chance that other pathologies, such as TAR DNA-binding protein of 43 kDA (TDP-43), are contributing to medial temporal volume loss (Josephs *et al.*, 2014, 2017).

Principal component analysis applied on longitudinal rates of tau accumulation and grey matter atrophy was still able to discriminate between Alzheimer's disease phenotypes, although revealing different patterns of variation compared to baseline measures. LPA participants were differentiated from typical Alzheimer's disease because they were characterized by higher annual rates of tau accumulation throughout the brain (PC1) and in the right temporoparietal lobe (PC4). PCA participants were differentiated from typical Alzheimer's disease and LPA for their higher rates of tau accumulation in the left lateral temporal and parietal regions and lower rates in the right occipital regions (PC3). PCA participants were also differentiated from the other two phenotypes in their rates of atrophy, showing higher rates in the occipital lobe, particularly on the right (PC3). From our principal component analysis results we could, therefore, infer that each Alzheimer's disease phenotype had its own pattern of baseline and rates of change in tau pathology and grey matter loss, with some overlap particularly in the temporoparietal regions. Others have suggested that, across Alzheimer's disease phenotypes, atrophy spreads to common regions as the disease progresses (Lehmann *et al.*, 2012; Ossenkoppele *et al.*, 2015) (e.g. temporoparietal), but it also maintains variant-specific trajectories, targeting those regions that are more vulnerable in each variant, i.e. language for LPA, visuo-spatial abilities for PCA and memory for typical amnestic Alzheimer's disease. Our results confirm this

hypothesis on MRI. Variant-specific trajectories were also observed on tau-PET, although in contrast to MRI, these trajectories did not target the same anatomical regions as atrophy, instead demonstrating spread to involve other regions of the brain. In general, all our analyses suggested that differences on imaging between Alzheimer's disease phenotypes are more striking cross-sectionally than longitudinally. However, principal component analysis was more capable to characterize longitudinal differences than traditional ROI- and voxel-based analyses.

The degree of disease severity, as quantified by the baseline MoCA score, was generally not related to the patterns of variability in images uncovered by the principal component analyses. The only exception was a mild correlation between MoCA and the first two principal components from cross-sectional MRI, which captured general severity and medial temporal volume loss, respectively. The relationships were identified in the expected direction, with worse clinical severity associated with smaller grey matter volumes.

The logistic regression models revealed that baseline tau uptake measurements outperformed the other modalities for their phenotype specificity using a limited number of principal components, being able to correctly classify a higher percentage of participants. More than 75% of participants were correctly classified using only the first four principal components. This suggests that baseline tau uptake best captures neurocognitive symptom variability in Alzheimer's disease. Others have found that flortaucipir PET uptake outperformed MRI measures in discriminating between Alzheimer's disease and other neurodegenerative disorders (Ossenkoppele *et al.*, 2018). The variability in tau-PET uptake is highly phenotype-specific while the variability in the other analysed imaging modalities, especially the longitudinal ones, has more common patterns across phenotypes reflecting future convergence to a common form of more severe dementia. A possible interpretation of our findings is that tau accumulation is not simply an intermediate in the pathway to loss of cortical volume. However, it is difficult to draw any conclusions on cause-effect mechanisms based solely on the current data and analyses. It is perhaps more likely that tau-PET uptake is a more sensitive measurement than MRI volumes in differentiating Alzheimer's disease phenotypes and hence it mirrors the clinical phenotypes more closely. A possible methodological limitation of our study is the use of SUVR to estimate longitudinal trajectories of tau-PET uptake. It has been recently demonstrated that the repeatability of SUVR measurements is good, but worsens in case of high baseline tau burden or low expected change over time (Timmers *et al.*, 2019). This aspect might have, to a certain extent, negatively impacted the ability of the longitudinal rates of tau-PET accumulation to discriminate between Alzheimer's disease phenotypes.

In our cohort of patients, there was a higher prevalence of *APOE* ε4 carriers in typical Alzheimer's disease compared to LPA and PCA participants, although the difference was statistically significant only with LPA. This is in accordance with previous studies that reported a lower prevalence of *APOE* ε4 carriers in aphasic versus amnestic dementias (Mesulam *et al.*, 1997; Rogalski *et al.*, 2011). Some have found a lower prevalence of *APOE* ε4 carriers in LPA compared to early-onset Alzheimer's disease and no differences in prevalence between LPA and PCA (Lehmann *et al.*, 2013), while others reported that the frequency of carriers across PCA, LPA and typical Alzheimer's disease differed (Phillips *et al.*, 2019). In general, it has been noted that *APOE* ε4 is less frequent in atypical Alzheimer's disease, affecting typical Alzheimer's disease more than the hippocampal-sparing phenotypes (Murray *et al.*, 2011; van der Flier *et al.*, 2011), with non-carriers characterized by higher atrophy in bilateral temporal, posterior parietal and occipital regions (Gutierrez-Galve *et al.*, 2009) and by less temporal tau-PET uptake (Ossenkoppele *et al.*, 2016).

A potential limitation of our study was the older age of the typical Alzheimer's disease group. This was by design in order to best represent true 'typical' amnestic Alzheimer's disease. However, it may limit generalizability of our findings to younger participants with amnestic Alzheimer's disease. The older age of the typical Alzheimer's disease participants is likely the reason why atrophy for this phenotype was circumscribed to the medial temporal lobe, with little involvement of the cortex. Pathological studies have shown that older age is associated with a more 'limbic-predominant' pattern of tau pathology in Alzheimer's disease (Murray *et al.*, 2011), and neuroimaging studies have similarly shown that older typical Alzheimer's disease subjects tend to have less involvement of the cortex (van der Flier *et al.*, 2011; Whitwell *et al.*, 2018*a*, 2019). Additionally, the clinical protocol was not identical for the typical and atypical Alzheimer's disease groups and this could limit the interpretation of the relationships between the neuroimaging biomarkers and the clinical progression. The inclusion of left-handed LPA participants might be controversial because a right instead of left lateralization of the disease has been reported in such patients (Mesulam *et al.*, 2014); however, in our cohort we did not observe any differences in laterality between left- and right-handed LPA participants. All our Alzheimer's disease participants had amyloid-β deposition observed on PET supporting the presence of underlying Alzheimer's disease pathology, although our cohort lacks autopsy confirmation and so we cannot rule out contributions from other co-pathologies. An advantage of principal component analysis is that it is an unsupervised technique, allowing us to assess variability in tau uptake and volumes unbiased by clinical diagnosis. Furthermore, we utilized penalization in our logistic regression models to reduce overfitting of the data and increase generalizability of the findings. However, our diagnostic accuracies will need to be validated in an independent sample. Baseline and longitudinal patterns of amyloid-PET uptake were not investigated since amyloid-β pathology is thought to start decades before the disease onset and, since the population of participants we analysed was at an advanced stage of the disease, amyloid was already widespread. Amyloid likely represents a biomarker more useful for early detection of Alzheimer's disease rather

than for discriminating across phenotypes and it may reveal phenotype-specific patterns with longer longitudinal datasets yet to be obtained.

Defining phenotype-specific biomarkers in Alzheimer's disease is important for inclusion as outcome measures in clinical treatment trials that enrol different clinical phenotypes of Alzheimer's disease. Our analyses may have implications for selecting the optimal biomarkers for Alzheimer's disease variants in both tau-PET and MRI. Our findings suggest that flortaucipir measures from the frontal lobe and MRI measures from the lateral temporal lobe are optimized longitudinal biomarkers for atypical Alzheimer's disease, while MRI measures from the medial temporal lobe would be the most appropriate longitudinal biomarkers for typical Alzheimer's disease.

Acknowledgements

We would like to greatly thank AVID Radiopharmaceuticals, Inc., for their support in supplying the AV-1451 precursor, chemistry production advice and oversight, and FDA regulatory cross-filing permission and documentation needed for this work.

Funding

This study was funded by National Institutes of Health grants R01-AG50603, R21-NS94684, P50-AG16574, R37-AG011378 and U01-AG006786.

Competing interests

J.L.W., K.A.J, C.G.S., M.M.M., D.T.J. and K.K. receive research support from the NIH. M.L.S. owns stock in Align Technology, Inc, Gilead Sciences, Inc., Globus Medical Inc., Inovio Biomedical Corp., Johnson & Johnson, LHC Group, Inc., Medtronic, Inc., Mesa Laboratories, Natus Medical Incorporated, Oncothyreon, Inc., Parexel International Corporation, Varex Imaging Corporation. B.F.B. has served as an investigator for clinical trials sponsored by Biogen and Alector; receives royalties from the publication of a book entitled Behavioral Neurology Of Dementia (Cambridge Medicine, 2017); serves on the Scientific Advisory Board of the Tau Consortium; receives research support from the NIH, the Mayo Clinic Dorothy and Harry T. Mangurian Jr. Lewy Body Dementia Program and the Little Family Foundation. D.S.K. serves on a Data Safety Monitoring Board for the DIAN study; is an investigator in clinical trials sponsored by Biogen, Lilly Pharmaceuticals and the University of Southern California; and receives research support from the NIH. R.C.P. is a consultant, adjudication committee or DSMB member for Roche, Inc., Merck, Inc., Genentech, Inc., Biogen, Inc., Eisai, Inc. and GE Healthcare. V.L. serves as a consultant for Bayer Schering Pharma, Philips Molecular Imaging, Piramal Imaging and GE Healthcare and receives research support from GE Healthcare, Siemens Molecular Imaging, AVID Radiopharmaceuticals, the NIH (NIA, NCI), and the MN Partnership for Biotechnology and Medical Genomics. C.R.J. serves on a scientific advisory board for Eli Lilly & Company, as a speaker for Eisai and on an independent data safety monitoring board for Roche but he receives no personal compensation from any commercial entity; receives research support from the NIH, and the Alexander Family Alzheimer's Disease Research Professorship of the Mayo Clinic.

Supplementary material

Supplementary material is available at *Brain* online.

References

Ashburner J, Friston KJ. Unified segmentation. Neuroimage 2005; 26: 839–51.

Avants BB, Epstein CL, Grossman M, Gee JC. Symmetric diffeomorphic image registration with cross-correlation: evaluating automated labeling of elderly and neurodegenerative brain. Med Image Anal 2008; 12: 26–41.

Braak H, Braak E. Neuropathological stageing of Alzheimer-related changes. Acta Neuropathol 1991; 82: 239–59.

Brambati SM, Amici S, Racine CA, Neuhaus J, Miller Z, Ogar J, et al. Longitudinal gray matter contraction in three variants of primary progressive aphasia: a tenser-based morphometry study. Neuroimage Clin 2015; 8: 345–55.

Chiotis K, Saint-Aubert L, Rodriguez-Vieitez E, Leuzy A, Almkvist O, Savitcheva I, et al. Longitudinal changes of tau PET imaging in relation to hypometabolism in prodromal and Alzheimer's disease dementia. Molecular Psychiatry 2018; 23: 1666–73.

Crutch SJ, Lehmann M, Schott JM, Rabinovici GD, Rossor MN, Fox NC. Posterior cortical atrophy. Lancet Neurol 2012; 11: 170–8.

Dronse J, Fliessbach K, Bischof GN, von Reutern B, Faber J, Hammes J, et al. In vivo patterns of tau pathology, amyloid-beta burden, and neuronal dysfunction in clinical variants of Alzheimer's Disease. J Alzheimers Dis 2017; 55: 465–71.

Firth NC, Primativo S, Marinescu RV, Shakespeare TJ, Suarez-Gonzalez A, Lehmann M, et al. Longitudinal neuroanatomical and cognitive progression of posterior cortical atrophy. Brain 2019; 142: 2082–95.

Frisoni GB, Testa C, Sabattoli F, Beltramello A, Soininen H, Laakso MP. Structural correlates of early and late onset Alzheimer's disease: voxel based morphometric study. J Neurol Neurosur Psychiatry 2005; 76: 112–4.

Galton CJ, Patterson K, Xuereb JH, Hodges JR. Atypical and typical presentations of Alzheimer's disease: a clinical, neuropsychological, neuroimaging and pathological study of 13 cases. Brain 2000; 123: 484–98.

Gollan TH, Weissberger GH, Runnqvist E, Montoya RI, Cera CM. Self-ratings of spoken language dominance: a Multilingual Naming Test (MINT) and preliminary norms for young and aging Spanish–English bilinguals. Bilingualism 2012; 15: 594–615.

Gorno-Tempini ML, Hillis AE, Weintraub S, Kertesz A, Mendez M, Cappa SF, et al. Classification of primary progressive aphasia and its variants. Neurology 2011; 76: 1006–14.

Gutierrez-Galve L, Lehmann M, Hobbs NZ, Clarkson MJ, Ridgway GR, Crutch S, et al. Patterns of Cortical Thickness according to APOE Genotype in Alzheimer's Disease. Dement Geriatr Cogn Disord 2009; 28: 476–85.

Harrison T M, La Joie R, Maass A, Baker S L, Swinnerton K, Fenton L, et al. Longitudinal tau accumulation and atrophy in aging and alzheimer disease. Ann Neurol 2019; 85: 229–40. 10.1002/ana.25406

Hughes CP, Berg L, Danziger WL, Coben LA, Martin RA. New clinical-scale for the staging of dementia. Br J Psychiatry 1982; 140: 566–72.

Ivnik RJ, Malec JF, Smith GE, Tangalos EG, Petersen RC, Kokmen E, et al. Mayo's older americans normative studies: Updated AVLT norms for ages 56 to 97. Clinical Neuropsychologist 1992; 6: 83–104.

Jack CR Jr, Lowe VJ, Senjem ML, Weigand SD, Kemp BJ, Shiung MM, et al. 11C PiB and structural MRI provide complementary information in imaging of Alzheimer's disease and amnestic mild cognitive impairment. Brain 2008; 131: 665–80.

Jack CR, Wiste HJ, Schwarz CG, Lowe VJ, Senjem ML, Vemuri P, et al. Longitudinal tau PET in ageing and Alzheimer's disease. Brain 2018; 141: 1517–28.

Jack CR, Wiste HJ, Weigand SD, Therneau TM, Lowe VJ, Knopman DS, et al. Defining imaging biomarker cut points for brain aging and Alzheimer's disease. Alzheimers Dement 2017; 13: 205–16.

Jolliffe I. Principal component analysis. New York: Springer; 1986. doi: 10.1007/978-1-4757-1904-8.

Jones DT, Graff-Radford J, Lowe VJ, Wiste HJ, Gunter JL, Senjem ML, et al. Tau, amyloid, and cascading network failure across the Alzheimer's disease spectrum. Cortex 2017; 97: 143–59.

Josephs KA, Dickson DW, Tosakulwong N, Weigand SD, Murray ME, Petrucelli L, et al. Rates of hippocampal atrophy and presence of post-mortem TDP-43 in patients with Alzheimer's disease: a longitudinal retrospective study. Lancet Neurol 2017; 16: 917–24.

Josephs KA, Martin PR, Botha H, Schwarz CG, Duffy JR, Clark HM, et al. [F-18]AV-1451 tau-PET and primary progressive aphasia. Ann Neurol 2018; 83: 599–611.

Josephs KA, Whitwell JL, Weigand SD, Murray ME, Tosakulwong N, Liesinger AM, et al. TDP-43 is a key player in the clinical features associated with Alzheimer's disease. Acta Neuropathol 2014; 127: 811–24.

Lansing AE, Ivnik RJ, Cullum CM, Randolph C. An empirically derived short form of the Boston Naming Test. Arch Clin Neuropsychol 1999; 14: 481–7.

Lehmann M, Barnes J, Ridgway GR, Ryan NS, Warrington EK, Crutch SJ, et al. Global gray matter changes in posterior cortical atrophy: a serial imaging study. Alzheimers Dement 2012; 8: 502–12.

Lehmann M, Ghosh PM, Madison C, Laforce R, Corbetta-Rastelli C, Weiner MW, et al. Diverging patterns of amyloid deposition and hypometabolism in clinical variants of probable Alzheimer's disease. Brain 2013; 136: 844–58.

Leow AD, Yanovsky I, Parikshak, N, Hua X, Lee S, Toga AW, et al. Alzheimer's Disease Neuroimaging Initiative: a one-year follow up study using tensor-based morphometry correlating degenerative rates, biomarkers and cognition. Neuroimage 2009; 45: 645–55.

Leuzy A, Cicognola C, Chiotis K, Saint-Aubert L, Lemoine L, Andreasen N, et al. Longitudinal tau and metabolic PET imaging in relation to novel CSF tau measures in Alzheimer's disease. Eur J Nucl Med Mol Imaging 2019; 46: 1152–63.

Lezak M, Howieson D, Loring D. Neuropsychological assessment. 5th edn. Oxford, New York: Oxford University Press; 2012.

Loonstra AS, Tarlow AR, Sellers AH. COWAT metanorms across age, education, and gender. Appl Neuropsychol 2001; 8: 161–6.

Lowe VJ, Wiste HJ, Senjem ML, Weigand SD, Therneau TM, Boeve BF, et al. Widespread brain tau and its association with ageing, Braak stage and Alzheimer's dementia. Brain 2018; 141: 271–87.

Machulda MM, Ivnik RJ, Smith GE, Ferman TJ, Boeve BF, Knopman D, et al. Mayo's older Americans normative studies: visual form discrimination and copy trial of the rey–osterrieth complex figure. J Clin Exp Neuropsychol 2007; 29: 377–84.

McKhann GM, Knopman DS, Chertkow H, Hyman BT, Jack CRJrKawas CH, et al. The diagnosis of dementia due to Alzheimer's disease: recommendations from the National Institute on Aging-Alzheimer's Association workgroups on diagnostic guidelines for Alzheimer's disease. Alzheimers Dement 2011; 7: 263–9.

Mesulam MM, Johnson N, Grujic Z, Weintraub S. Apolipoprotein E genotypes in primary progressive aphasia. Neurology 1997; 49: 51–5.

Mesulam MM, Rogalski EJ, Wieneke C, Hurley RS, Geula C, Bigio EH, et al. Primary progressive aphasia and the evolving neurology of the language network. Nat Rev Neurol 2014; 10: 554–69.

Murray ME, Graff-Radford NR, Ross OA, Petersen RC, Duara R, Dickson DW. Neuropathologically defined subtypes of Alzheimer's disease with distinct clinical characteristics: a retrospective study. Lancet Neurol 2011; 10: 785–96.

Nasreddine ZS, Phillips NA, Bedirian V, Charbonneau S, Whitehead V, Collin I, et al. The Montreal cognitive assessment, MoCA: a brief screening tool for mild cognitive impairment. J Am Geriatr Soc 2005; 53: 695–9.

Ossenkoppele R, Cohn-Sheehy BI, La Joie R, Vogel JW, Moller C, Lehmann M, et al. Atrophy patterns in early clinical stages across distinct phenotypes of Alzheimer's disease. Hum Brain Mapp 2015; 36: 4421–37.

Ossenkoppele R, Rabinovici GD, Smith R, Cho H, Scholl M, Strandberg O, et al. Discriminative accuracy of [F-18]flortaucipir Positron Emission Tomography for Alzheimer disease vs other neurodegenerative disorders. JAMA 2018; 320: 1151–62.

Ossenkoppele R, Schonhaut DR, Scholl M, Lockhart SN, Ayakta N, Baker SL, et al. Tau PET patterns mirror clinical and neuroanatomical variability in Alzheimer's disease. Brain 2016; 139: 1551–67.

Osterrieth P. Le test de copie d'une figure complexe: contribution à l'étude de l'aperception et de la mémoire. Arch Psychol 1944; 30: 205–353.

Pagani M, Salmaso D, Rodriguez G, Nardo D, Nobili F. Principal component analysis in mild and moderate Alzheimer's disease - A novel approach to clinical diagnosis. Psychiatry Res 2009; 173: 8–14.

Phillips JS, Da Re F, Dratch L, Xie SX, Irwin DJ, McMillan CT, et al. Neocortical origin and progression of gray matter atrophy in non-amnestic Alzheimer's disease. Neurobiol Aging 2018; 63: 75–87.

Phillips JS, Da Re F, Irwin DJ, McMillan CT, Vaishnavi SN, Xie SX, et al. Longitudinal progression of grey matter atrophy in non-amnestic Alzheimer's disease. Brain 2019; 142: 1701–22.

Pontecorvo MJ, Devous MD, Kennedy I, Navitsky M, Lu M, Galante N, et al. A multicentre longitudinal study of flortaucipir (F-18) in normal ageing, mild cognitive impairment and Alzheimer's disease dementia. Brain 2019; 142: 1723–35.

Raz L, Jayachandran M, Tosakulwong N, Lesnick TG, Wille SM, Murphy MC, et al. Thrombogenic microvesicles and white matter hyperintensities in postmenopausal women. Neurology 2013; 80: 911–8.

Rey A. L'examen clinique en psychologie, Paris: presses Universitaires de France. Chemother Obj Cogn Funct 1958; 95: 1964.

Roberts RO, Geda YE, Knopman DS, Cha RH, Pankratz VS, Boeve BF, et al. The Mayo Clinic Study of Aging: design and sampling, participation, baseline measures and sample characteristics. Neuroepidemiology 2008; 30: 58–69.

Rogalski EJ, Rademaker A, Harrison TM, Helenowski I, Johnson N, Bigio E, et al. ApoE E4 is a susceptibility factor in amnestic but not aphasic dementias. Alzheimer Dis Assoc Disord 2011; 25: 159–63.

Rogalski EJ, Sridhar J, Martersteck A, Rader B, Cobia D, Arora AK, et al. Clinical and cortical decline in the aphasic variant of Alzheimer's disease. Alzheimers Dement 2019; 15: 543–52.

Rohrer JD, Caso F, Mahoney C, Henry M, Rosen HJ, Rabinovici G, et al. Patterns of longitudinal brain atrophy in the logopenic variant of primary progressive aphasia. Brain Lang 2013; 127: 121.6.

Scahill RI, Schott JM, Stevens JM, Rossor MN, Fox NC. Mapping the evolution of regional atrophy in Alzheimer's disease: unbiased analysis of fluid-registered serial MRI. Proc Natl Acad Sci USA 2002; 99: 4703–7.

Scholl M, Ossenkoppele R, Strandberg O, Palmqvist S, Jogi J, Ohlsson T, et al. Distinct F-18-AV-1451 tau PET retention patterns in early- and late-onset Alzheimer's disease. Brain 2017; 140: 2286–94.

Schwarz CG, Gunter JL, Ward CP, Vemuri P, Senjem ML, Wiste HJ, et al. The mayo clinic adult life span template: better quantification across the life span. Alzheimers Dement 2017; 13: P93–P4.

Sintini I, Martin PR, Graff-Radford J, Senjem ML, Schwarz CG, Machulda MM, et al. Longitudinal tau-PET uptake and atrophy in atypical Alzheimer's disease. Neuroimage Clin 2019; 23: 101823.

Sintini I, Schwarz CG, Martin PR, Graff-Radford J, Machulda MM, Senjem ML, et al. Regional multimodal relationships between tau, hypometabolism, atrophy, and fractional anisotropy in atypical Alzheimer's disease. Hum Brain Mapp 2018;

Tetzloff KA, Graff-Radford J, Martin PR, Tosakulwong N, Machulda MM, Duffy JR, et al. Regional distribution, asymmetry, and clinical correlates of tau uptake on [18F]AV-1451 PET in Atypical Alzheimer's disease. J Alzheimers Dis 2018; 62: 1713–24.

Timmers T, Ossenkoppele R, Visser D, Tuncel H, Wolters EE, Verfaillie SC, et al. Test–retest repeatability of [18F] Flortaucipir PET in Alzheimer's disease and cognitively normal individuals. J Cereb Blood Flow Metab 2019; 0271678X19879226.

van der Flier WM, Pijnenburg YA, Fox NC, Scheltens P. Early-onset versus late-onset Alzheimer's disease: the case of the missing APOE ε4 allele. Lancet Neurol 2011; 10: 280–8.

Vemuri P, Senjem ML, Gunter JL, Lundt ES, Tosakulwong N, Weigand SD, et al. Accelerated vs. unaccelerated serial MRI based TBM-SyN measurements for clinical trials in Alzheimer's disease. Neuroimage 2015; 113: 61–9.

Vogel JW, Mattsson N, Iturria-Medina Y, Strandberg OT, Scholl M, Dansereau C, et al. Data-driven approaches for tau-PET imaging biomarkers in Alzheimer's disease. Hum Brain Mapp 2019; 40: 638–51.

Whitwell JL, Graff-Radford J, Tosakulwong N, Weigand SD, Machulda M, Senjem ML, et al. [F-18]AV-1451 clustering of entorhinal and cortical uptake in Alzheimer's disease. Ann Neurol 2018a; 83: 248–57.

Whitwell J L, Graff-Radford J, Tosakulwong N, Weigand S D, Machulda M M, Senjem M L, et al. Imaging correlations of tau, amyloid, metabolism, and atrophy in typical and atypical Alzheimer's disease. Alzheimer's & Dementia 2018; 14: 1005–14. 10.1016/j.jalz.2018.02.020

Whitwell JL, Jack CR, Kantarci K, Weigand SD, Boeve BF, Knopman DS, et al. Imaging correlates of posterior cortical atrophy. Neurobiol Aging 2007a; 28: 1051–61.

Whitwell JL, Jack CR, Przybelski SA, Parisi JE, Senjem ML, Boeve BF, et al. Temporoparietal atrophy: a marker of Alzheimer's disease pathology independent of clinical diagnosis. Neurobiol Aging 2011; 32: 1531–41.

Whitwell JL, Martin P, Graff-Radford J, Machulda MM, Senjem ML, Schwarz CG, et al. The role of age on tau PET uptake and gray matter atrophy in atypical Alzheimer's disease. Alzheimers Dement 2019; 15: 675–85.

Whitwell JL, Przybelski SA, Weigand SD, Knopman DS, Boeve BF, Petersen RC, et al. 3D maps from multiple MRI illustrate changing atrophy patterns as subjects progress from mild cognitive impairment to Alzheimer's disease. Brain 2007b; 130: 1777–86.

Xia C, Makaretz SJ, Caso C, McGinnis S, Gomperts SN, Sepulcre J, et al. Association of in vivo [18F]AV-1451 Tau PET imaging results with cortical atrophy and symptoms in typical and Atypical Alzheimer disease. JAMA Neurol 2017; 74: 427–36.

Xia MR, Wang JH, He Y. BrainNet viewer: a network visualization tool for human brain connectomics. Plos One 2013; 8: e68910. doi: 10.1371/journal.pone.0068910.

Zuendorf G, Kerrouche N, Herholz K, Baron JC. Efficient principal component analysis for multivariate 3D voxel-based mapping of brain functional imaging data sets as applied to FDG-PET and normal aging. Hum Brain Mapp 2003; 18: 13–21.